The trapped two-dimensional Bose gas: from Bose-Einstein condensation to Berezinskii-Kosterlitz-Thouless physics

Z. Hadzibabic[1,2], P. Krüger[1,3,4], M. Cheneau[1], S. P. Rath[1] and J. Dalibard[1]

[1] Laboratoire Kastler Brossel, CNRS, École normale supérieure, 24 rue Lhomond, 75005 Paris

[2] Cavendish Laboratory, University of Cambridge, Cambridge CB3 0HE, United Kingdom

[3] Kirchhoff Institut für Physik, Universität Heidelberg, 69120 Heidelberg, Germany

[4] Midlands Centre for Ultracold Atoms, School of Physics and Astronomy, University of Nottingham, Nottingham NG7 2RD, United Kingdom.

E-mail: `jean.dalibard@lkb.ens.fr`

Abstract. We analyze the results of a recent experiment with bosonic rubidium atoms harmonically confined in a quasi-two-dimensional geometry. In this experiment a well defined critical point was identified, which separates the high-temperature normal state characterized by a single component density distribution, and the low-temperature state characterized by a bimodal density distribution and the emergence of high-contrast interference between independent two-dimensional clouds. We first show that this transition cannot be explained in terms of conventional Bose-Einstein condensation of the trapped ideal Bose gas. Using the local density approximation, we then present a hybrid approach, combining the mean-field (MF) Hartree-Fock theory with the prediction for the Berezinskii-Kosterlitz-Thouless transition in an infinite uniform system. We compare the MF results with those of a recent Quantum Monte-Carlo (QMC) analysis. For the considered experiment, both approaches lead to a strong and similar correction to the critical atom number with respect to the ideal gas theory (factor ~ 2). The spatial density profiles obtained using the QMC method significantly deviate from the MF prediction, and a similar deviation is observed in the experiment. This suggests that beyond mean-field effects can play a significant role at the critical point in this geometry. A quantitative agreement between theory and experiment can be reached concerning the critical atom number if the QMC results are used for temperature calibration.

1. Introduction

As first noticed by Peierls [1], collective physical phenomena in an environment with a reduced number of dimensions can be dramatically changed with respect to our experience in three dimensions. The example of Bose-Einstein condensation in a uniform gas is a good illustration of the crucial role of dimensionality. In three dimensions (3D), condensation occurs at a finite temperature, and the phase of the macroscopic wave function exhibits long range order [2]. In two dimensions, such long range order is destroyed by thermal fluctuations at any finite temperature, both for an ideal and for an interacting Bose gas [3, 4].

In presence of repulsive interactions between particles, a uniform 2D Bose gas can nevertheless undergo a phase transition from a normal to a superfluid state at a finite critical temperature. This transition was predicted by Berezinskii [5] and by Kosterlitz and Thouless [6] (BKT), and it has been observed in several macroscopic quantum systems, such as helium films adsorbed on a substrate [7]. The superfluid state exhibits quasi-long range order, such that the one-body correlation function decays algebraically at large distance. By contrast the decay is exponential in the normal phase.

The recent advances in the manipulation of quantum atomic gases have made it possible to address the properties of low-dimensional Bose gases with novel tools and diagnostic techniques [8, 9, 10, 11, 12, 13, 14, 15, 16, 17, 18]. (for recent reviews, see [19, 20]). A recent cold atom experiment also addressed the BKT problem by realizing a two-dimensional array of atomic Josephson junctions [21]. All these systems bring new questions, since one is now dealing with a harmonically trapped, instead of a uniform, fluid. In particular, due to a different density of states, even in 2D one expects to recover the Bose-Einstein condensation phenomenon in the ideal Bose gas case [22]. The total number of atoms in the excited states of the trap is bounded from above, and a macroscopic population of the ground state appears for large enough atom numbers. However real atomic gases do interact. It is therefore a challenging question to understand whether in presence of atomic interactions, a trapped Bose gas will undergo a BKT superfluid transition like in the uniform case, or whether conventional Bose-Einstein condensation will take place, as for an ideal system.

In recent experiments performed in our laboratory [17, 18], a gas of rubidium atoms was trapped using a combination of a magnetic trap providing harmonic confinement in the xy plane, and an optical lattice, ensuring that the third degree of freedom (z) of the gas was frozen. The analysis of the atomic density profile revealed a critical point, between a high temperature phase with a single component density distribution, and a low temperature phase with a clear bimodal distribution [18]. This critical point also corresponded to the onset of clearly visible interferences between independent gases, which were used to study the coherence properties of the system [17]. Surprisingly, the density profile of the normal component was observed to be close to a gaussian all the way down (in temperature) to the critical point. This density profile is strikingly different from the one expected for the ideal gas close to the BEC critical temperature.

Furthermore, if the width of the observed quasi-gaussian distribution is interpreted as an empirical measure of the temperature, this leads to a critical atom number at a given temperature which is about five times larger than that needed for the conventional Bose-Einstein condensation in the ideal gas. These two facts showed that, in sharp contrast to the 3D case, interactions in 2D cannot be treated as a minor correction to the ideal gas BEC picture, but rather qualitatively change the behavior of the system.

The main goal of the present paper is to analyze this critical point. We start by giving a detailed comparison with the predictions for an ideal gas. In § 2 we give a brief review of the properties of an ideal Bose gas in the uniform case and in the case of harmonic confinement. In § 3 we adapt the ideal gas treatment to the experimental geometry of [18], and provide a detailed calculation showing that the experimental results cannot be explained by this theory. Next, we show that taking interactions into account at the mean-field level is also insufficient to fully account for the experimental results. In § 4 we combine a mean-field analysis for a trapped gas with the numerically known threshold for the BKT transition in the uniform case [23]. Although the results obtained in this way are much closer to the experimental findings than the ideal gas theory, the calculated density profiles are still clearly distinguishable from the experimentally observed ones. We also compare our experimental results with the most recent Quantum Monte Carlo (QMC) calculations [24]. These calculations indeed give a quasi-gaussian density distribution of the normal component near the critical point, and a critical density in the center of the trap which agrees with the BKT threshold in a uniform system. They also show that the "empirical" temperature extracted from the quasi-gaussian distribution is in fact somewhat lower than the real temperature. Taking this into account we obtain good quantitative agreement between our experimental results and the QMC calculations, and conclude that BKT behavior and beyond mean-field effects were observed in our experiments. Finally we summarize our findings and discuss the connection between the BEC and the BKT transition in a 2D gas. While in a uniform, infinite system only the latter can occur at a finite temperature, in a trapped gas both are possible, and the BEC transition can be viewed as a special, non-interacting limit of the more general BKT behavior.

2. Bose-Einstein condensation in an ideal 2D Bose gas

This section is devoted to a review of well known results concerning the ideal Bose gas in two dimensions. We first address the case of a uniform system at the thermodynamic limit, and we then consider a gas confined in a harmonic potential.

2.1. The uniform case

In the thermodynamic limit a uniform, ideal Bose gas does not undergo Bose-Einstein condensation when the temperature T is reduced, or the 2D spatial density n is increased. Bose-Einstein statistics leads to the following relation between the phase

space density $D = n\lambda^2$ and the fugacity $Z = \exp(\beta\mu)$

$$D = g_1(Z) , \qquad g_\alpha(Z) = \sum_{j=1}^{\infty} Z^j/j^\alpha . \tag{1}$$

Here $\lambda = \hbar(2\pi/(mk_BT))^{1/2}$ is the thermal wavelength, m is the atomic mass, $\beta = 1/(k_BT)$ and μ is the chemical potential. The function $g_\alpha(Z)$ is the polylogarithm, that takes the simple form $g_1(Z) = -\ln(1-Z)$ for $\alpha = 1$. Because $g_1(Z) \to +\infty$ when $Z \to 1$, (1) has a solution in Z for any value of D. Hence no singularity appears in the distribution of the population of the single particle levels, even when the gas is strongly degenerate $(D \gg 1)$. This is to be contrasted with the well known 3D case: the relation $D^{(3D)} = g_{3/2}(Z)$ ceases to have a solution for a phase space density above the critical value $D_c^{(3D)} = g_{3/2}(1) \simeq 2.612$, where the 3D Bose-Einstein condensation phenomenon takes place.

2.2. The ideal 2D Bose gas in a harmonic confinement

We now consider an ideal gas confined in a harmonic potential $V(\mathbf{r}) = m\omega^2r^2/2$. We assume that thermal equilibrium has been reached, so that the population of each energy level is given by Bose-Einstein statistics. Since the chemical potential μ is always lower than the energy $\hbar\omega$ of the ground state of the trap, the number of atoms N' occupying the excited states of the trap cannot exceed the critical value $N_c^{(id)}$

$$N_c^{(id)} = \sum_{j=1}^{+\infty} \frac{j+1}{\exp(j\beta\hbar\omega) - 1} . \tag{2}$$

This expression can be evaluated in the so-called *semi-classical limit* $k_BT \gg \hbar\omega$ by replacing the discrete sum by an integral over the energy ranging from 0 to $+\infty$ [22]:

$$N_c^{(id)} = \left(\frac{k_BT}{\hbar\omega}\right)^2 g_2(1) , \tag{3}$$

with $g_2(1) = \pi^2/6$. This result also holds in the case of an anisotropic harmonic potential in the xy plane, in which case ω is replaced by the geometric mean $\bar\omega = \sqrt{\omega_x\omega_y}$, where ω_x, ω_y are the two eigenfrequencies of the trap. The saturation of the number of atoms in the excited states is a direct manifestation of Bose-Einstein condensation: any total atom number N above $N_c^{(id)}$ must lead to the accumulation of at least $N - N_c^{(id)}$ in the ground state of the trap.

Equation (3) is very reminiscent of the result for the harmonically trapped 3D gas, where the saturation number is $N_c^{(3D,id)} = (k_BT/(\hbar\omega))^3 g_3(1)$. However an important difference arises between the 2D and the 3D cases for the spatial density profile. In 3D the phase space density in $\mathbf{r}$ is given by $D^{(3D)}(\mathbf{r}) = g_{3/2}(Ze^{-\beta V(\mathbf{r})})$ in the limit $k_BT \gg \hbar\omega$. The threshold for Bose-Einstein condensation is reached for $Z = 1$; at this point N is equal to the critical number $N_c^{(3D,id)}$ and simultaneously the phase space density at the center of the trap $D^{(3D)}(0)$ equals the critical value $g_{3/2}(1)$. This allows for a simple connection between the BEC thresholds for a homogenous gas and for a trapped system in the semi-classical limit $k_BT \gg \hbar\omega$. In 2D such a simple connection between global

properties (critical atom number $N_c^{(id)}$) and local properties (critical density at center $n(0)$) does not exist. Indeed the semi-classical expression of the 2D phase space density is

$$D(\mathbf{r}) = g_1(Ze^{-\beta V(\mathbf{r})}) . \tag{4}$$

Because $g_1(1) = +\infty$ this leads to a diverging value at the center of the trap when Z approaches 1. Therefore, although the integral of $D(\mathbf{r})$ over the whole space converges for $Z = 1$ and allows to recover (3), the semiclassical result (4) cannot be used to derive a local criterion for condensation at the center of the trap.

One can go beyond the semi-classical approximation and calculate numerically the central phase space density as a function of the total number of atoms. We consider as an example the trap parameters used in [18], where $\omega_x/(2\pi) = 9.4$ Hz, $\omega_y/(2\pi) = 125$ Hz. In the typical case $k_B T/(\hbar\bar{\omega}) = 50$ ($T \simeq 80$ nK), the discrete summation of the Bose-Einstein occupation factors for $Z = 1$ gives $N_c \simeq 4800$ (the value obtained from the semi-classical result (3) is 4100). Using the expression of the energy eigenstates (Hermite functions), we also calculate the phase space density at the origin and we find $D(0) \simeq 13$. Let us emphasize that this value is a mere result of the finite size of the system, and does not have any character of universality.

3. Condensation of an ideal Bose gas in a harmonic + periodic potential

In order to produce a quasi two-dimensional gas experimentally, one needs to freeze the motion along one direction of space, say z. In practice this is conveniently done using the potential $V^{(lat)}(z) = V_0 \sin^2(kz)$ created by an optical lattice along this direction. A precise comparison between the measured critical atom number and the prediction for an ideal gas requires to properly model the confining potential and find its energy levels. This is the purpose of the present section.

3.1. The confining potential

The optical lattice is formed by two running laser waves of wavelength λ, propagating in the yz plane with an angle $\pm\theta/2$ with respect to the y axis. The period $\ell = \pi/k = \lambda/(2\sin(\theta/2))$ of the lattice along the z direction can be adjusted to any value above $\lambda/2$ by a proper choice of the angle θ. For a blue-detuned lattice (λ is smaller than the atomic resonance wavelength), V_0 is positive and the atoms accumulate in the vicinity of the nodal planes $z = 0$, $z = \pm\pi/k$, etc. The oscillation frequency at the bottom of the lattice wells is $\omega_z^{(lat)} = 2\sqrt{V_0 E_r}/\hbar$, where $E_r = \hbar^2 k^2/(2m)$. In order for the quasi-2D regime to be reached, $\hbar\omega_z^{(lat)}$ must notably exceed the typical thermal energy $k_B T$ as well as the interaction energy per particle for a non ideal gas.

For a blue detuned lattice an additional confinement in the xy plane must be added to the optical lattice potential. This is conveniently achieved using a magnetic trap, that creates a harmonic potential with frequencies ω_x, ω_y. The magnetic trap also provides an additional trapping potential $m\omega_z^2 z^2/2$ along the z direction. The oscillation frequency

ω_z created by the magnetic trap is usually much lower than the one created by the lattice $\omega_z^{(\text{lat})}$. The main effect of the magnetic confinement along the z direction is to localize the atoms in the $\mathcal{N}$ central lattice planes, where the effective number of planes $\mathcal{N} \sim 4\, k_B T/(m\omega_z^2 \ell^2)$. As we see below this number is on the order of 2 to 4 for the range of parameters explored in [18]. The fact that more than just one plane is populated is an important ingredient of the experimental procedure used in [17, 18]. It allows one to look for the interferences between planes, and to access in this way the spatial coherence of the quasi-2D gas.

In order to extract thermodynamic information from the interference between planes, one must ensure that the various populated planes have the same temperature. This is achieved by using finite size lattice beams in the xy plane, so that atoms in the high energy tail of the thermal distribution can actually travel quasi freely from one plane to the other, thus ensuring thermalization. In the experiments described in [17, 18], the waist W_x of the lattice beams along the x direction was chosen accordingly. The total trapping potential can then be written in the following way

$$V(\mathbf{r}) = V^{(\text{mag})}(\mathbf{r}) + V^{(\text{lat})}(\mathbf{r}) \tag{5}$$

with

$$V^{(\text{mag})}(\mathbf{r}) = \frac{1}{2}m\left(\omega_x^2 x^2 + \omega_y^2 y^2 + \omega_z^2 z^2\right) \tag{6}$$

$$V^{(\text{lat})}(\mathbf{r}) = V_0\, e^{-2x^2/W_x^2}\, \sin^2(k(z-z_0)) \tag{7}$$

Note that we have included here the offset z_0 between the optical lattice and the bottom of the magnetic potential; this quantity was not set to a fixed value in the experiments [17, 18]. We consider below two limiting situations: (A) $kz_0 = \pi/2$, with two principal equivalent minima in $kz = \pm\pi/2$, (B) $kz_0 = 0$, with one principal minimum in $z = 0$ and two side minima in $kz = \pm\pi$. At very low temperatures, we expect that A will lead to two equally populated planes whereas configuration B will lead to one populated plane. For the temperature range considered in practice, the differences between the predictions for A and B are minor, as we will see below.

3.2. Renormalization of the trapping frequency ω_x by the optical lattice

In order to use the Bose-Einstein statistics for an ideal gas, one needs to know the position of the single particle energy levels. For the potential (5) it is not possible to find an exact analytical expression of these levels. However if the extension of the atomic motion along the x direction remains small compared to the laser waist, an approximate expression can be readily obtained, as we show now.

The frequencies of the magnetic trap used in [17, 18] are $\omega_x = 2\pi \times 10.6$ Hz and $\omega_y = \omega_z = 2\pi \times 125$ Hz. The optical lattice has a period $\pi/k = 3$ μm ($E_r = \hbar^2 k^2/(2m) = h \times 80$ Hz) and a potential height at center $U_0/h = 35$ kHz (1.7 μK). The lattice oscillation frequency at center ($x = 0$) is thus $\omega_z^{(\text{lat})}(x = 0) = 2\pi \times 3$ kHz ($\hbar\omega_z^{(\text{lat})}/k_B = 150$ nK). When the atoms occupy the ground state of the z motion, they acquire the zero-point energy $\hbar\omega_z^{(\text{lat})}(x)/2$ from the $z-$degree of freedom. The

dependance on x of $\omega_z^{(\mathrm{lat})}(x)$, due to the gaussian term e^{-2x^2/W_x^2} in the laser intensity, causes a renormalization of the x frequency:

$$\omega_x^2 \to \omega'^2_x = \omega_x^2 - \frac{2\sqrt{V_0 E_r}}{mW_x^2} \ . \tag{8}$$

The waist of the lattice beams is $W_x = 120\,\mu$m which leads to $\omega'_x = 2\pi \times 9.4$ Hz. A similar effect should in principle be taken into account for the frequency ω_y. However the scale of variation of the laser intensity along the y axis is the Rayleigh length, which is much larger than the waist W_x, and the effect is negligible.

This simple way of accounting for the finiteness of the waist W_x is valid when the extension of the motion along x is small compared to W_x. For $T = 100$ nK, the width of the thermal distribution along x is $\sqrt{k_B T/m\omega_x^2} \sim 50\,\mu$m, which is indeed notably smaller than W_x. Taking into account the finiteness of W_x by a mere reduction of the trapping frequency along x is therefore valid for the major part of the energy distribution.

We note however that atoms in the high energy tail of the distribution ($E > 5\,k_B T$ for our largest temperatures) can explore the region $|x| > W_x$, where the influence of the lattice beams is strongly reduced. In this region the atoms can move from one lattice plane to the other. As explained above these atoms play an important role by ensuring full thermalization between the various planes. We now turn to an accurate treatment of the critical atom number required for Bose-Einstein condensation, taking into account these high energy levels for which the 2D approximation is not valid.

3.3. The critical atom number in a 'Born–Oppenheimer' type approximation

In order to get the single particle energy eigenstates in the lattice + harmonic potential confinement, and thus the critical atom number, one could perform a numerical diagonalization of the 3D hamiltonian with the potential (5). This is however a computationally involved task and it is preferable to take advantage of the well separated energy scales in the problem.

We first note that the trapping potential (5) is the sum of a term involving the variables x and z, and a quadratic component in y. The motion along the y axis can then be separated from the xz problem, and it is easily taken into account thanks to its harmonic character. For treating the xz problem we use a 'Born-Oppenheimer' type approximation. We exploit the fact that the characteristic frequencies of the z motion are in any point x notably larger than the frequency of the x motion. This is of course true inside the lattice laser waist, since $\omega_z^{(\mathrm{lat})}/\omega_x \sim 300$, and it is also true outside the laser waist as the x direction corresponds to the weak axis of our magnetic trap. Therefore we can proceed in two steps:

 (i) For any fixed x we numerically find the eigenvalues $E_j(x)$, $j = 0, 1, \ldots$ of the z motion in the $(V^{(\mathrm{mag})} + V^{(\mathrm{lat})})(x, z)$ potential. We determine the E_j's up to the threshold $6\,k_B T$ above which the thermal excitation of the levels is negligible. The result of this diagonalization is shown in figure 1 for configurations A and B.
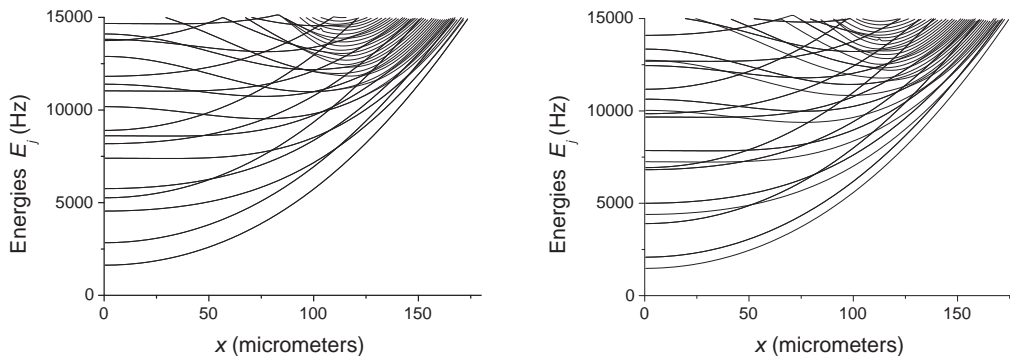
Figure 1. Eigenvalues of the z-motion in the magnetic+optical $x - z$ potential, for fixed values of the x coordinate (left: configuration A, right: configuration B).

(ii) We then treat semi-classically the x-motion on the various potential curves $E_j(x)$. Adding the result for the independent harmonic y motion –also treated semi-classically– we obtain the surface density $n(x, y)$ (integral of the spatial density $n_3(\mathbf{r})$ along the direction z)

$$n(x, y) = \frac{1}{\lambda^2} \sum_j g_1 \left(Z e^{-\beta(E_j(x) + V^{(\mathrm{mag})}(y))} \right) \ . \tag{9}$$

This procedure yields a result that is identical to the semi-classical prediction in two limiting cases:

 (i) The pure 2D case, that is recovered for large waists and low temperatures. In this case the restriction to the closest-to-center lattice plane and to the first z-level is legitimate, and the sum over j contains only one significant term corresponding to (4).

(ii) the pure 3D harmonic case with zero lattice intensity where $E_j(x) = m\omega_x^2 x^2/2 + (j + 1/2)\hbar\omega_z$. In this case the sum over j in (9) leads to $n(x, y)\ \lambda^2 = g_2 \left(Z e^{-\beta V^{(\mathrm{mag})}(x,y)} \right) / (\beta\hbar\omega_z)$, which coincides with the 3D result $D^{(\mathrm{3D})}(\mathbf{r}) = g_{3/2}(Z e^{-\beta V(\mathbf{r})})$ when integrated along z.

Of course this procedure also allows to interpolate between these two limiting cases, which is the desired outcome. The integral of n in the xy plane for $\mu = \min\left(E_j(x) + V^{(\mathrm{mag})}(y)\right)$ gives the critical atom number $N_c^{(\mathrm{lat,id})}(T)$ in the ideal gas model for this lattice geometry. It is shown in figure 2a for the two configurations A and B.

The critical atom number $N_c^{(\mathrm{lat,id})}$ can be compared with the result for a single plane $N_c^{(\mathrm{id})}$ with eigenfrequencies ω_x' and ω_y. The ratio gives the effective number of planes $\mathcal{N}_{\mathrm{eff}}$, shown as a function of temperature in figure 2b for the two configurations A and B. This ratio increases with temperature, which means that $N_c^{(\mathrm{lat,id})}$ increases faster than T^2 with temperature in the temperature domain considered here. For example in the range $50 - 110$ nK, the variation of $N_c^{(\mathrm{lat,id})}$ is well represented by T^β, with $\beta = 2.8$.

Three phenomena contribute significantly to this "faster than T^2" increase of $N_c^{(\text{lat,id})}$. First in the lattice + harmonic potential geometry, the number of contributing planes increases with temperature, even if the atomic motion in each plane remains two-dimensional (i.e. the atom number per plane increasing strictly as T^2). Second, we are exploring here a region of temperature where $k_B T$ becomes non negligible with respect to $\hbar\omega_z^{(\text{lat})}$ (the two quantities are equal for $T = 150$ nK), and the thermal excitations of the z-motion in each lattice plane cannot be fully neglected. Third, for the largest considered temperatures, the extension of the atomic motion along x becomes comparable to the laser waist, and the lattice strength is then significantly reduced.
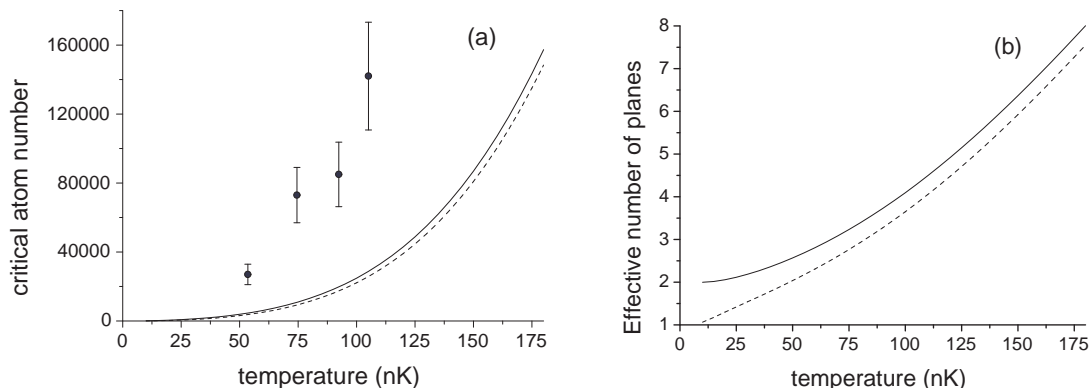

Figure 2. (a) Critical atom number $N_c^{(\text{lat,id})}$ in the ideal gas model for the optical lattice + magnetic trap configuration, as a function of temperature. The points represent the experimental results of [18], and the error bars combine the systematic and statistical uncertainties on atom numbers. (b) Effective number of planes $\mathcal{N}_{\text{eff}} = N_c^{(\text{lat,id})}/N_c^{(\text{id})}$ as a function of temperature. In both panels the continuous (dashed) curve is for configuration A (B). The calculation is performed using the first 100 eigenvalues of the z motion, and the first neglected levels $E_j(x)$ are 22 kHz (1 μK) above the bottom of the trap.

3.4. Comparison with experimental results

In [18] the critical atom number in the lattice + magnetic trap configuration was measured for various "effective" temperatures, deduced from the width of the quasi-gaussian atomic distribution. Each critical point $(N_c^{(\text{exp})}, T_c^{(\text{exp})})$ was defined as the place where a bimodal spatial distribution appeared, if the atom number was increased beyond this point at constant temperature, or the temperature reduced at constant atom number. The critical point also corresponded to the threshold for the appearance of interferences with a significant contrast between adjacent planes. The experimental measurements of critical points, taken over the effective temperature range 50–110 nK, are shown as dots in figure 2a. The systematic + statistical uncertainties of the atom number calibration is 25%. Assuming that the effective temperatures coincide with the true ones (this point will be examined in § 4.5) we find $N_c^{(\text{exp})}/N_c^{(\text{lat,id})} \sim 5.3$ (± 1.2).

In addition to this large discrepancy between experiment and ideal gas model for the critical atom numbers, one also finds a strong mismatch concerning the functional shape of the column density $\int n(x,y)dy$ that was measured in absorption imaging in [17, 18]. While the experimental result is quasi-gaussian, the column density profiles calculated for an ideal gas at the critical point are much 'peakier'. An example is given in the appendix for a single plane, and we checked that a similar shape remains valid for our harmonic + lattice potential. We therefore conclude that the experimental results of [18] cannot be accounted for with this ideal gas prediction for 'conventional' BEC.

4. Interactions in a 2D trapped Bose gas

To improve the agreement between the experimental results and the theoretical modeling we now take repulsive atomic interactions into account. For simplicity we will not consider in this section the lattice geometry of the experiment, but rather restrict ourselves to a single 2D atomic plane. In order to model interactions in a quasi-2D gas, we start from the 3D interaction energy $(g^{(3D)}/2) \int n_3^2(\mathbf{r}) \, d^3r$, where $g^{(3D)} = 4\pi\hbar^2 a/m$ and a is the scattering length. We assume that the z-motion is restricted to the gaussian ground state of the confining potential ‡, with an extension $a_z = \sqrt{\hbar/(m\omega_z^{(\text{lat})})}$, and we obtain the interaction energy

$$E_{\text{int}} = \frac{g}{2} \int n^2(\mathbf{r}) \, d^2r \ .$$

We set $g = \hbar^2 \tilde{g}/m$, where the dimensionless parameter $\tilde{g} = \sqrt{8\pi}\, a/a_z$ characterizes the strength of the 2D interaction (for a more elaborate treatment of atomic interactions in a quasi-2D geometry, see [25, 26]). For the optical lattice used in [18] we find $\tilde{g} = 0.13$.

4.1. Criticality within mean-field solutions: 3D vs. 2D

We shall start our discussion with a brief reminder of the role of (weak) interactions in a trapped 3D Bose gas [27]. One often uses the mean field Hartree-Fock approximation, that gives in particular a relatively accurate value for the shift of the critical temperature for Bose-Einstein condensation. In order to calculate this shift, one assumes that above the critical temperature, the atoms evolve in the effective potential $V_{\text{eff}}(\mathbf{r}) = V(\mathbf{r}) + 2g^{(3D)}n_3(\mathbf{r})$. The phase space density in $\mathbf{r}$ is thus a solution of $D^{(3D)}(\mathbf{r}) = g_{3/2}(Ze^{-\beta V_{\text{eff}}(\mathbf{r})})$. As for the ideal case this equation ceases to have a solution when the central phase space density goes above $g_{3/2}(1)$. The mere effect of repulsive interactions within the mean field approximation is to increase the number of atoms for which this threshold is met. The increase is typically $\sim 10\%$ for standard trap and interaction parameters [27].

For a trapped 2D gas this treatment based on a local criterion (phase space density at center) cannot be used. Indeed as explained in section 2.2, it is not possible to identify a critical phase space density at which BEC of the 2D gas is expected. On the contrary

‡ The consequences of small deviations to this approximation are discussed in [24].

the semiclassical approximation leads to an infinite central density at the critical point, and it is unclear whether one can achieve an arbitrarily large spatial density in presence of repulsive interactions.

One could also look for a global criterion for criticality based on the total atom number. The starting point is the solution of the mean-field equation

$$D(\mathbf{r}) = g_1 \left(Z e^{-\beta V_{\text{eff}}(\mathbf{r})} \right) \tag{10}$$

with $V_{\text{eff}}(\mathbf{r}) = V(\mathbf{r}) + 2g\, n(\mathbf{r})$. When $g = 0$, we saw in §2 that the solution of (10) can only accommodate a finite number of atoms (3). However the situation is dramatically changed in presence of repulsive interactions. Indeed for any non zero g, a solution to (10) exists for arbitrarily large atom numbers [28]. Consequently no critical point can be found by simply searching for a maximal atom number compatible with (10). In the following we will therefore turn to a different approach, starting from the known exact (i.e. non mean-field) results concerning the critical BKT point in a uniform interacting 2D Bose gas. The mean-field approximation will be used in a second stage, in combination with the local density approximation (LDA), to determine the critical atom number in the trapped system.

We would like to note that it is also possible to pursue the search for a critical point only within the mean-field approach, by looking for example whether its solution exhibits a thermodynamical or dynamical instability above a critical atom number [29, 30]. This instability is an indication that the system tends to evolve towards a different kind of state, with a non-zero quasi-condensed and/or superfluid component, and quasi-long range order [31, 32].

4.2. The Berezinskii-Kosterlitz-Thouless transition and the local density approximation

In an infinite uniform 2D Bose fluid, repulsive interactions have a dramatic effect since they can induce a transition from the normal to the superfluid state, when the temperature is lowered below a critical value. The superfluid density jumps from 0 to $4/\lambda^2$ at the transition point [33]. The microscopic mechanism of the 2D superfluid transition has been elucidated by Berezinskii [5] and by Kosterlitz and Thouless [6]. For a temperature larger than the critical temperature, free vortices proliferate in the gas, destroying the superfluidity. Below the transition, vortices exist only in the form of bound pairs involving two vortices of opposite circulations, which have little influence on the superfluid properties of the system.

In a uniform system the phase space density D is a function of the chemical potential and temperature $D = F(\mu, T)$. For any given T, the superfluid transition occurs when μ is equal to a critical value $\mu_c(T)$. The corresponding critical value D_c for the phase space density depends on the interaction strength as [34, 35, 36]

$$D_c = \ln(\xi/\tilde{g}) \tag{11}$$

where ξ is a dimensionless number. A recent Monte-Carlo analysis provided the result $\xi = 380 \pm 3$ [23] (see also [37]). For $\tilde{g} = 0.13$ this gives a critical phase space density $D_c = 8.0$.
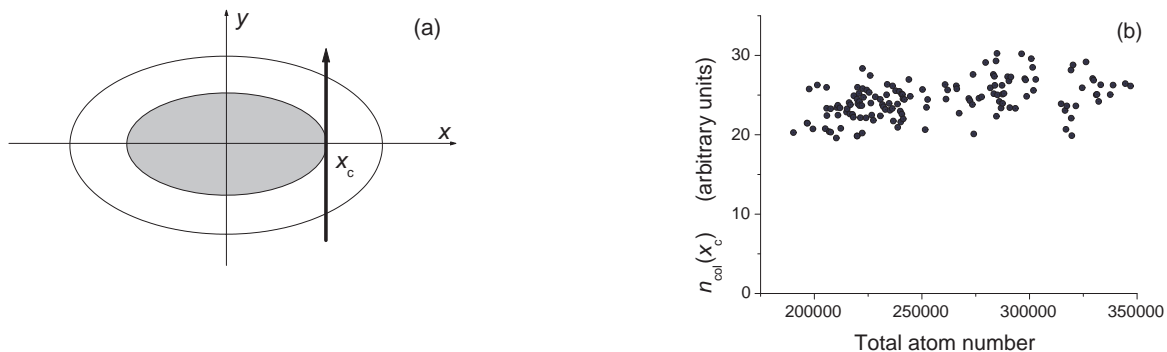
Figure 3. Check of the local density approximation (LDA). (a) The column density n_{col} is measured at the edge $x = x_{\mathrm{c}}$ of the central part (in grey) of the bimodal distribution. (b) $n_{\mathrm{col}}(x_{\mathrm{c}})$ is plotted as a function of the total atom number N in the harmonic trap + lattice configuration. Within the LDA for a single plane, $n_{\mathrm{col}}(x_{\mathrm{c}})$ should be independent of N, which is indeed nearly the case. The small variation of $n_{\mathrm{col}}(x_{\mathrm{c}})$ for large N may be due to the appearance of a non negligible population in side planes of the optical lattice potential. The data have been taken for $T = 105$ nK. Each point is extracted from a single image.

We consider now a trapped gas whose size is large enough to be well described by the local density approximation (LDA). The phase space density in $\mathbf{r}$ is given by $D(\mathbf{r}) = F(\mu - V(\mathbf{r}), T)$ and a superfluid component forms around the center of the trap if the central phase density $D(0)$ is larger than D_{c} [38]. The edge of the superfluid region corresponds to the critical line where $\mu - V(\mathbf{r}) = \mu_{\mathrm{c}}$. The phase space density along this line is equal to D_{c}, independently of the total number of atoms in the trap. This can be checked experimentally and constitutes a validation of the LDA. The integration of the experimental data along the line of sight y does not lead to any complication because the trapping potential is separable $V(\mathbf{r}) = V_1(x) + V_2(y)$. Therefore the edges of the superfluid region along the x axis are located in $\pm x_{\mathrm{c}}$ such that $V_1(x_{\mathrm{c}}) = \mu - \mu_{\mathrm{c}}$ (see figure 3a), and the column density along the line of sight passing in $x = x_{\mathrm{c}}$ is

$$n_{\mathrm{col}}(x_{\mathrm{c}}) = \frac{1}{\lambda^2} \int D(x_{\mathrm{c}}, y)\, dy = \frac{1}{\lambda^2} \int F(\mu_{\mathrm{c}} - V_2(y), T)\, dy \tag{12}$$

which is also independent of the total atom number N. This is confirmed experimentally, as shown in figure 3b where we plot $n_{\mathrm{col}}(x_{\mathrm{c}})$ as a function of N. The slight increase (10%) of $n_{\mathrm{col}}(x_{\mathrm{c}})$ for atom numbers larger than 3×10^5 may be due to the fact that the population of additional planes becomes non-negligible for such large N.

4.3. Density profile in the mean field approximation

In this section we use the mean field Hartree-Fock approximation (10) to calculate the density profile of the trapped atomic cloud. As we mentioned above, this equation admits a solution for any value of the fugacity Z, and therefore for an arbitrarily large

number of particles. Rewriting (10) as

$$D(\mathbf{r}) = -\ln\left(1 - Ze^{-\tilde{g}D(\mathbf{r})/\pi}e^{-\beta V(\mathbf{r})}\right) \tag{13}$$

we see that the value of D for any temperature and at any point in space depends only on the parameter R defined by $R^2 = (x/x_T)^2 + (y/y_T)^2$, where $x_T = (\omega_x^2 m\beta)^{-1/2}$ and $y_T = (\omega_y^2 m\beta)^{-1/2}$. The total atom number is given by

$$N = \left(\frac{k_B T}{\hbar\bar{\omega}}\right)^2 \int_0^\infty \tilde{D}(R)\, R\, dR \tag{14}$$

where $\tilde{D}(R)$ is the solution of the reduced equation

$$\tilde{D}(R) = -\ln\left(1 - Ze^{-\tilde{g}\tilde{D}(R)/\pi}e^{-R^2/2}\right)\ . \tag{15}$$

Quite remarkably this result for $\tilde{D}(R)$ does not depend on the trap parameters, nor on the temperature. The only relevant parameters are the fugacity Z and the reduced interaction strength $\tilde{g}$. The scaling of the atom number N with the temperature and the trap frequency in (14) is therefore very simple. In particular it does not depend on the trap anisotropy ω_y/ω_x but only on the geometric mean $\bar{\omega}$.

As an example we show in figure 4a the density profile $D(r)$ for an atom number equal to the critical value found in the ideal case (3). The length unit is $r_T = (\omega^2 m\beta)^{-1/2}$. We have also indicated in this figure the semi-classical result $g_1(e^{-\beta V(r)})$ for the ideal Bose gas. The latter is diverging in $r = 0$, as explained in section 2. For $r > 0.5\, r_T$ the mean-field and the ideal gas solutions nearly coincide. §

For atom numbers much larger than $N_c^{(\mathrm{id})}$ it is interesting to note that the radial density profile deduced from the mean-field equation (13) exhibits a clear bi-modal shape, with wings given by $n(r)\lambda^2 \simeq Ze^{-\beta V(\mathbf{r})}$ and a central core with a Thomas-Fermi profile $2g\,n(r) \simeq \mu - V(\mathbf{r})$. However this prediction of a bi-modal distribution using the Hartree-Fock approximation cannot be quantitatively correct. Indeed the Hartree-Fock treatment assumes a mean field energy $2gn$. The factor 2 in front of this energy originates from the hypothesis that density fluctuations are those of a gaussian field $\langle n^2\rangle = 2\langle n\rangle^2$. Actually when the phase space density becomes significantly larger than 1, density fluctuations are reduced and one approaches a situation closer to a quasi-condensate in which $\langle n^2\rangle \sim \langle n\rangle^2$ [23]. Taking into account this reduction could be done for example using the equation of state obtained from a classical field Monte-Carlo analysis in [39] .

4.4. Critical atom number in the mean field approximation

We now use the solution of the mean-field equation (13) to evaluate the critical atom number $N_c^{(\mathrm{mf})}$ that is needed to reach the threshold (11) for the BKT transition at

§ We have also investigated the density profile predicted using the equation of state obtained from a classical field Monte-Carlo analysis [39]. The predictions of this analysis (not plotted in figure 4) nearly coincide with the mean-field result for a phase space density below 4 ($X \leq -2$ using the notations of [39]), which is indeed the case at any point in space for the parameters of figure 4a.
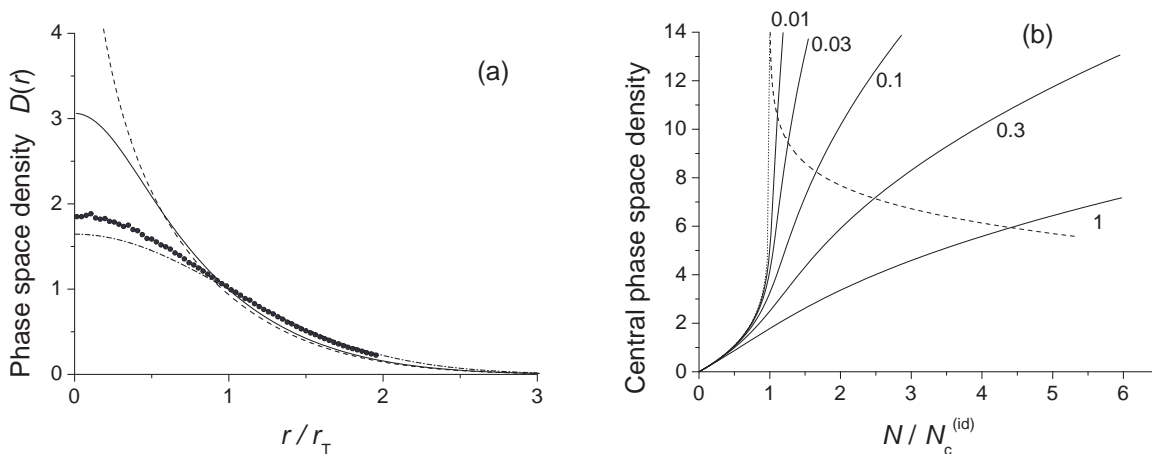
Figure 4. (a) Radial phase space density for $N = N_c^{(\mathrm{id})}$. Full line: mean-field result with $\tilde{g} = 0.13$; dashed line: semi-classical result for an ideal gas; dash-dotted line: gaussian distribution corresponding to the Boltzmann law $\exp(-r^2/(2r_T^2))$. The result of the quantum Monte-Carlo obtained in [24] is plotted as dots, and is close to the gaussian result. (b) Central phase space density as a function of the atom number for various interaction strengths $\tilde{g}$. The dotted line represents the semi-classical prediction for the ideal gas. The dashed line indicates where the threshold for superfluidity (11) is met at the center of the trap.

the center of the trap $D(0) = \ln(\xi/\tilde{g})$. For a given interaction strength $\tilde{g}$ we vary the fugacity Z, solve numerically (13) at any point in space, and then calculate the total atom number N. From (14) and (15), it is clear that the scaling of $N_c^{(\mathrm{mf})}$ with the frequencies $\omega_{x,y}$ and with the temperature is identical to the one expected for an ideal trapped gas.

We have plotted in figure 4b the variation of $D(0)$ as a function of $N/N_c^{(\mathrm{id})}$ for various interaction strengths. For a given atom number the phase space density at center decreases when the strength of the interactions increases, as expected. The numerical result for $N_c^{(\mathrm{mf})}$ is plotted as a dashed line in figure 4b. We find that it is in excellent agreement – to better than 1%– with the result of [38]

$$\frac{N_c^{(\mathrm{mf})}}{N_c^{(\mathrm{id})}} = 1 + \frac{3\tilde{g}}{\pi^3}D_c^2 \tag{16}$$

over the whole range $\tilde{g} = 0-1$. This analytical result was initially derived in [38] for $g \ll 1$ using an expansion around the solution for the ideal Bose gas, but this approximation can actually be extended to an arbitrary value of $\tilde{g}$ [40]. The strongly interacting limit $(3\tilde{g}D_c^2/\pi^3 > 1)$ can be easily understood by noticing that in this case, the atomic distribution (10) nearly coincides with the Thomas-Fermi profile $2gn(r) = \mu - V(r)$. Using the relation between the total atom number and the central density for this Thomas-Fermi distribution $N = 2\pi\tilde{g}\left(n(0)a_{\mathrm{ho}}^2\right)^2$ (with $a_{\mathrm{ho}} = (\hbar/(m\omega))^{1/2}$), one then recovers the second term of the right-hand side of (16).

Let us emphasize that figure 4b is a mix of two approaches: (i) The mean-field model, that does not lead in itself to a singularity along the dashed line of figure 4b. (ii) The BKT theory for a uniform system, which is a beyond mean-field treatment and which has been adapted to the trapped case using the local density approximation in order to obtain the critical number indicated by the dashed line.

4.5. Mean-field vs. Quantum Monte-Carlo predictions

Recently Holzmann and Krauth [24] performed a quantum Monte-Carlo (QMC) analysis of a 2D Bose gas with parameters similar to the experimental values of [18]. Since the QMC results are 'exact' (within statistical errors) it is interesting to use them in order to estimate the quality of the mean-field predictions.

The first test concerns the atomic density profile. We have plotted in figure 4a the density profile obtained numerically by Holzmann and Krauth for $N = N_c^{(id)}$. Quite remarkably the QMC result is close to the "Boltzmann gaussian result" $(\pi^2/6)\, e^{-\beta V(r)}$. This is not the case for the mean field prediction, which leads for this atom number to a larger central phase space density and smaller wings than the QMC prediction. The quasi-gaussian character of the QMC prediction is worth noting since the density profiles measured experimentally are also close to gaussian, as long as the atom number is smaller than the critical value.

The second test concerns the critical atom number for a given temperature. The mean field prediction obtained from (16) for $\tilde{g} = 0.13$ is $N_c^{(mf)}/N_c^{(id)} = 1.8$. This is in good agreement with the QMC calculation of [24], which gives $T_c^{(QMC)} = 0.70\, T_c^{(id)}$ or equivalently $N_c^{(QMC)}/N_c^{(id)} = 2.0$. It is important to note that the mean-field and QMC spatial distributions at the critical point are notably different, although they correspond to the same central phase space density D_c. (i) Just around the center of the trap, the mean-field theory leads to a density peak whose width is larger than the QMC result. This originates from the already discussed factor 2 appearing in the interaction energy ($2gn$ instead of gn), that should not be present in the central region where density fluctuations are strongly suppressed. (ii) The density in the wings of the atomic distribution predicted by the mean-field theory is on the contrary lower than the QMC result, as pointed out above for the data of figure 4a.

4.6. Comparison with experimental results

We finally compare the experimental results of [18] with the predictions of the mean field and QMC approaches, starting with the density profiles. As already mentioned the observed density profiles are close to a gaussian distribution, as long as the critical point has not been reached. This is consistent with the results of the QMC treatment [24] (see figure 4a), and notably different from the predictions of the mean-field approach. The fact that the experiment is performed after a time-of-flight does not change this mismatch between the mean-field prediction and the experimental results, as shown in the appendix.

The QMC result can be used to calibrate more accurately the temperature in the experiment. In [18] the effective temperature was determined by a fit of the atomic spatial distribution with the Boltzmann law $e^{-V(\mathbf{r})/kT}$. The same procedure can be applied to the QMC distributions close to the critical point, and it shows that the effective temperature extracted from the fit is smaller than the real one by a factor $\eta = 0.77\,(\pm 0.07)$.

We now turn to the comparison between theory and experiment concerning the critical atom number at which bimodality and local coherence appear. In § 3.4 the experimentally measured critical atom number $N_{\mathrm{c}}^{(\mathrm{exp})}$ was found to be larger than the prediction $N_{\mathrm{c}}^{(\mathrm{lat,id})}$ for an ideal gas by a factor $N_{\mathrm{c}}^{(\mathrm{exp})}/N_{\mathrm{c}}^{(\mathrm{lat,id})} = 5.3\,(\pm 1.2)$. Now we have just seen that the BKT threshold at the center of a single 2D trap is reached for $N_{\mathrm{c}}^{(\mathrm{QMC})}/N_{\mathrm{c}}^{(\mathrm{id})} = 2.0$, which is much smaller than the experimental factor 5.3. However we also mentioned that the gaussian fit that was performed on the experimental data underestimated the temperature by a factor $\eta = 0.77$. As $N_{\mathrm{c}}^{(\mathrm{lat,id})}$ varies as $T^{2.8}$ (see § 3.3), this recalibration of the temperature gives the corrected ratio $N_{\mathrm{c}}^{(\mathrm{exp})}/N_{\mathrm{c}}^{(\mathrm{lat,id})} = 2.6\,(\pm 0.8)$. This ratio is consistent with both QMC and mean-field predictions. To improve on the precision of this check it is clear that a more controlled experimental setup is needed, with an accurate independent measurement of temperature, as well as the possibility of addressing only a fixed number of planes.

5. Summary and concluding remarks

In this paper we have analyzed the critical point of a trapped 2D Bose gas. We have shown that the experimental results of [18] are not in agreement with the ideal Bose gas theory. The differences are found first at the qualitative level: the predicted shape for the ideal gas distribution is 'peaky' around its center, which clearly differs from the quasi-gaussian measured profile. Also the measured critical atom numbers $N_{\mathrm{c}}(T)$ do not agree with the predictions for the ideal gas. Using the 'effective' temperatures obtained by treating the gaussian profiles as Boltzmann distributions, the measured $N_{\mathrm{c}}(T)$ are larger by a factor ~ 5.3 than the predicted ones. We then discussed the predictions of a hybrid approach based on the local density approximation. It combines the density profile calculated using a mean-field Hartree-Fock treatment, and the known result for the critical phase space density for the BKT transition in an infinite, uniform 2D Bose gas [23]. We compared the predictions of this approach with the results of a recent Quantum Monte-Carlo calculation [24]. For the experimental parameters of [18] both approaches give a strong and similar correction to the ideal gas result $N_c \sim 2\,N_{\mathrm{c}}^{(\mathrm{id})}$. The spatial density profiles predicted by the QMC analysis near the critical point are close to a gaussian distribution, like those measured experimentally. The density profiles obtained from the Hartree-Fock method significantly deviate from the QMC ones, which suggests that beyond mean-field effects can play a significant role at the critical point for this quasi-2D geometry. A good agreement between theory (both QMC and mean-field) and experiment is reached concerning the critical number $N_c(T)$ when the QMC density
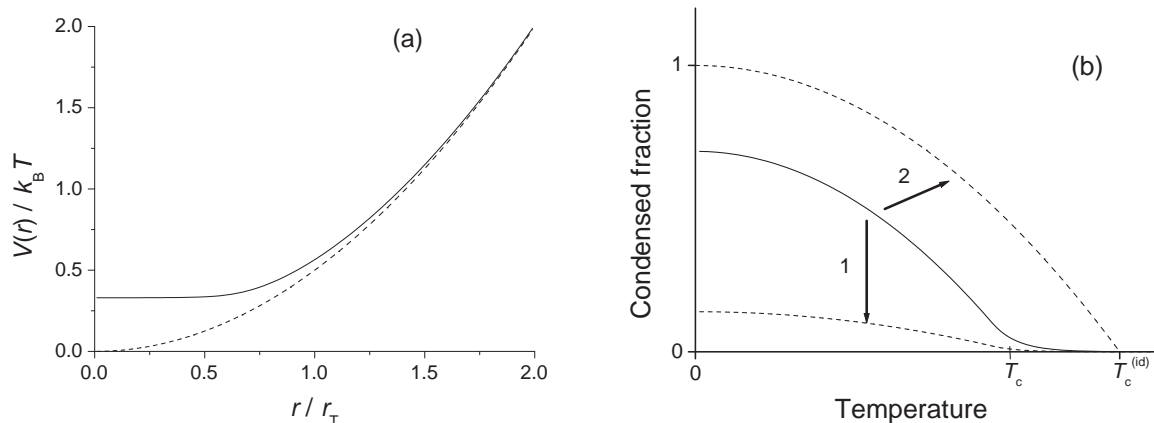
Figure 5. (a) Trapping potential $V(r)$ in dashed line and effective mean-field potential $V_{\mathrm{eff}}(r) = V(r)+2gn(r)$ in continuous line, for $\tilde{g} = 0.13$ and a central phase space density equal to the critical value (11). (b) Schematic representation of the condensed fraction in a finite 2D Bose gas for a given interaction strength $\tilde{g}$ (continuous line). Two limits can be considered: (1) thermodynamic limit $N \to \infty$, $\omega \to 0$, $N\omega^2$ constant; the condensed fraction tends to zero for any non zero value of $\tilde{g}$. (2) ideal gas limit $\tilde{g} \to 0$.

profile is used for temperature calibration.

We now briefly discuss the nature of the critical point that appears in the trapped 2D Bose gas and compare it with 'standard' Bose-Einstein condensation. For a harmonically trapped ideal gas, we recall that conventional Bose-Einstein condensation is expected in the thermodynamic limit $N \to \infty$, $\omega \to 0$, $N\omega^2$ constant. This is a consequence of the density of states for a quadratic hamiltonian around the zero energy. The 'price to pay' for this condensation in a 2D system is a diverging atomic density at the center of the trap. On the contrary when interactions are taken into account, the mean-field approximation leads to the potential $V(\mathbf{r}) + 2gn(\mathbf{r})$ that is flat at the origin (figure 5a and [38]). The 'benefit' of the harmonic trapping potential is lost and the physics of the trapped interacting gas is very similar to that of a uniform system. In particular one expects in the thermodynamic limit the appearance of quasi-long range order only, with no true Bose-Einstein condensate [25]. ‖ The transition between the ideal and the interacting case is explicit in equations (11) and (16), where the limit $\tilde{g} \to 0$ gives $D_{\mathrm{c}} \to +\infty$ and $N_{\mathrm{c}}^{(\mathrm{mf})}/N_{\mathrm{c}}^{(\mathrm{id})} \to 1$. In particular (16) can be used to separate a 'BEC-dominated' regime where $\eta = 3\tilde{g}D_{\mathrm{c}}^2/\pi^3 \ll 1$ and $N_{\mathrm{c}} \simeq N_{\mathrm{c}}^{(\mathrm{id})}$, and a 'BKT-dominated' regime, where the contribution of η is dominant and $N_{\mathrm{c}} \gg N_{\mathrm{c}}^{(\mathrm{id})}$. In the latter case, the spatial distribution in the mean-field approximation is a Thomas-Fermi disk with radius R_{TF} and (16) is equivalent (within a numerical factor) to the BKT threshold (11) for a uniform gas with density $n = N/(\pi R_{\mathrm{TF}}^2)$. The rubidium gas studied in [17, 18] is at the border of the 'BKT-dominated' regime ($\eta \simeq 1$), whereas previous experiments

‖ A similar flattening of the mean-field potential occurs in 3D, but it has no important consequence in this case since true BEC is possible in an infinite, uniform 3D system.

performed on quasi-2D gases of sodium atoms [8] corresponded to $\eta \sim 0.1$, well inside the 'BEC-dominated' regime.

Finally, we must take into account the finite size of the gas in our discussion. It is known from simulations of 2D spin assemblies that for a finite size system, the average magnetization increases rapidly around the BKT transition [41]. It is at first sight surprising that this magnetization can be used as a signature of BKT physics, since it would not exist in an infinite system where a genuine BKT transition takes place. However it is relevant for all practical 2D situations: as emphasized in [41] one would need extremely large systems ('bigger than the state of Texas') to avoid a significant magnetization even just below the transition point. A similar phenomenon occurs for a finite size Bose gas. A few states acquire a large population around the transition point, and this allows for the observation of good contrast interferences between two independent gases. In particular the condensed fraction f_0 (largest eigenvalue of the one-body density matrix) is expected to grow rapidly at the critical point, and this has been quantitatively confirmed by the QMC calculation of [24]. To illustrate this point we have schematically plotted in figure 5b the expected variations of f_0 with the parameters of the problem. For given $\tilde{g}$ and N, f_0 takes significant values for $T < T_{\rm c}$ (continuous line). If the strength of the interactions $\tilde{g}$ is kept constant, the condensed fraction f_0 tends to zero for any finite temperature if the thermodynamic limit is taken (arrow 1 in figure 5b). Note that the superfluid fraction should tend to a finite value in this limiting procedure. Now one can also keep N constant and decrease $\tilde{g}$ to zero (arrow 2 in figure 5b). In this case one expects to recover the ideal gas result $f_0 = 1 - (T/T_{\rm c}^{({\rm id})})^2$ for any value of N. Therefore we are facing here a situation where two limits do not commute: $\lim_{N\to\infty} \lim_{g\to0} \neq \lim_{g\to0} \lim_{N\to\infty}$. Of course this does not cause any problem in practice since none of these limits is reached. In this sense the phenomenon observed in our interacting, trapped 2D Bose gas is hybrid: the transition point is due to BKT physics (the density of states of the ideal 2D harmonic oscillator does not play a significant role because of the flattening of the potential), but thanks to the finite size of the system, some diagnoses of the transition such as the appearance of interferences, take benefit of the emergence of a significant condensed fraction.

Acknowledgments

Appendix: The time-of-flight in the mean field approximation

An important result of this paper is the deviation of the measured density profiles from those calculated for an ideal gas or using the mean-field approximation. The profiles calculated in steady-state in the trap are found much 'peakier' than the experimental ones. As the experimental profiles were actually measured after a time of flight of $t = 22$ ms ($\omega_x t = 1.3$), it is important to check that this mismatch between predicted and observed profiles remain valid when the ballistic expansion of the atoms is taken into account. Also the atom distributions were measured using an absorption imaging technique, with an imaging beam propagating along the y axis. Therefore the measurement gave access to the column density $n_{\text{col}}(x,t)$, obtained by integrating the total density along y. In this appendix we take into account the time-of-flight and the integration along the y direction, both for an ideal and for an interacting gas within the mean-field approximation.

The spatial distribution $n(\mathbf{r},t)$ at time t can be calculated from the phase space distribution $\rho(\mathbf{r},\mathbf{p})$ at initial time using

$$n(\mathbf{r},t) = \int \rho(\mathbf{r} - \mathbf{p}t/m, \mathbf{p}) \, d^2p \ . \tag{A.1}$$

In the semi-classical approximation the in-trap phase space density is given by

$$\rho(\mathbf{r},\mathbf{p}) = \frac{1}{h^2} \left\{ \exp\left[\left(p^2/(2m) + V_{\text{eff}}(\mathbf{r}) - \mu \right) / k_B T \right] - 1 \right\}^{-1} , \tag{A.2}$$

where $V_{\text{eff}} = V(\mathbf{r}) + 2gn(\mathbf{r})$, and $n(\mathbf{r})$ is obtained by solving (13). The result for the column density can be written

$$n_{\text{col}}(x,t) = \frac{1}{x_T} \left(\frac{k_B T}{\hbar \omega} \right)^2 F(X,Z,\tilde{g},\tau) \ , \quad X = \frac{x}{x_T} \ , \quad \tau = \omega_x t. \tag{A.3}$$

The results for F are shown in figure A1a for an ideal gas, and in figure A1b for an interacting gas in the mean field approximation. In the ideal gas case, the initial column density can be calculated analytically :

$$F(X,Z,0,0) = \frac{1}{\sqrt{2\pi}} \, g_{3/2}\left(Z e^{-X^2/2} \right) \tag{A.4}$$

and the column density after time of flight is deduced from the initial value by a simple dilatation

$$F(X,Z,0,\tau) = \frac{1}{\sqrt{1+\tau^2}} F\left(\frac{X}{\sqrt{1+\tau^2}}, Z, 0, 0 \right) \ . \tag{A.5}$$

In figure A1a, the fugacity is such that the atom number equals the critical number (3). In the interacting case of figure A1b, the number of atoms is such that the criterion for superfluidity is met at the center of the trap. In all cases, it is clear that the observed profiles are very different from a gaussian, in clear disagreement with the experimental observation.

[1] R. E. Peierls. *Ann. Inst. Henri Poincaré*, 5:177, 1935.

[2] O. Penrose and L. Onsager. Bose-Einstein condensation and liquid helium. *Phys. Rev.*, 104:576, 1956.
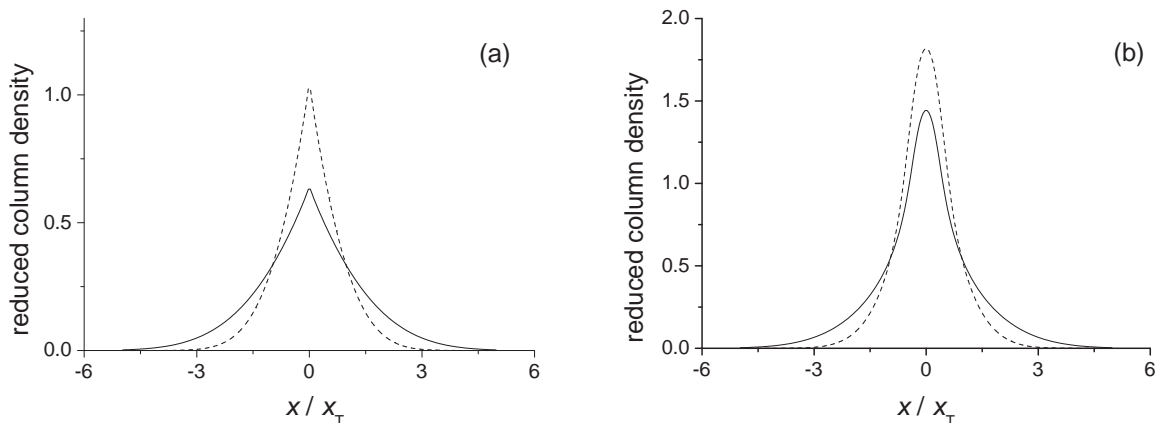
Figure A1. Reduced column density F in the trap (dashed line) and after a time of flight t such that $\omega_x t = 1.3$ (continuous line). (a) Ideal gas case, for an atom number equal to the critical value (3). (b) Mean field result for $\tilde{g} = 0.13$. The fugacity is chosen such that the threshold for superfluidity (11) is met at the center of the trap.

[3] P. C. Hohenberg. Existence of long-range order in one and two dimensions. *Phys. Rev.*, 158:383, 1967.

[4] N. D. Mermin and H. Wagner. Absence of ferromagnetism or antiferromagnetism in one- or two-dimensional isotropic Heisenberg models. *Phys. Rev. Lett.*, 17:1307, 1966.

[5] V. L. Berezinskii. Destruction of long-range order in one-dimensional and two-dimensional system possessing a continous symmetry group - ii. quantum systems. *Soviet Physics JETP*, 34:610, 1971.

[6] J. M. Kosterlitz and D. J. Thouless. Ordering, metastability and phase transitions in two dimensional systems. *J. Phys. C: Solid State Physics*, 6:1181, 1973.

[7] D. J. Bishop and J. D. Reppy. Study of the superfluid transition in two-dimensional ^{4}He films. *Phys. Rev. Lett.*, 40(26):1727–1730, Jun 1978.

[8] A. Görlitz, J. M. Vogels, A. E. Leanhardt, C. Raman, T. L. Gustavson, J. R. Abo-Shaeer, A. P. Chikkatur, S. Gupta, S. Inouye, T. Rosenband, and W. Ketterle. Realization of Bose-Einstein condensates in lower dimensions. *Phys. Rev. Lett.*, 87:130402, 2001.

[9] D. Rychtarik, B. Engeser, H.-C. Nägerl, and R. Grimm. Two-dimensional Bose-Einstein condensate in an optical surface trap. *Phys. Rev. Lett.*, 92:173003, 2004.

[10] N. L. Smith, W. H. Heathcote, G. Hechenblaikner, E. Nugent, and C. J. Foot. Quasi-2D confinement of a BEC in a combined optical and magnetic potential. *Journal of Physics B*, 38:223, 2005.

[11] Y. Colombe, E. Knyazchyan, O. Morizot, B. Mercier, V. Lorent, and H. Perrin. Ultracold atoms confined in rf-induced two-dimensional trapping potentials. *Europhys. Lett*, 67:593, 2004.

[12] S. Burger, F. S. Cataliotti, C. Fort, P. Maddaloni, F. Minardi, and M. Inguscio. Quasi-2D Bose-Einstein condensation in an optical lattice. *Europhys. Lett.*, 57:1, 2002.

[13] M. Köhl, H. Moritz, T. Stöferle, C. Schori, and T. Esslinger. Superfluid to Mott insulator transition in one, two, and three dimensions. *Journal of Low Temperature Physics*, 138:635, 2005.

[14] C. Orzel, A. K. Tuchmann, K. Fenselau, M. Yasuda, and M. A. Kasevich. Squeezed states in a Bose-Einstein condensate. *Science*, 291:2386, 2001.

[15] I. B. Spielman, W. D. Phillips, and J. V. Porto. The Mott insulator transition in two dimensions. *Phys. Rev. Lett.*, 98:080404, 2007.

[16] Z. Hadzibabic, S. Stock, B. Battelier, V. Bretin, and J. Dalibard. Interference of an array of

independent Bose-Einstein condensates. *Phys. Rev. Lett.*, 93:180403, 2004.

[17] Z. Hadzibabic, P. Krüger, M. Cheneau, B. Battelier, and J. Dalibard. Berezinskii-Kosterlitz-Thouless crossover in a trapped atomic gas. *Nature*, 441:1118–1121, May 2006.

[18] P. Krüger, Z. Hadzibabic, and J. Dalibard. Critical point of an interacting two-dimensional atomic Bose gas. *Phys. Rev. Lett.*, 99(4):040402, 2007.

[19] A. Posazhennikova. Weakly interacting, dilute Bose gases in 2D. *Rev. Mod. Phys.*, 78:1111, 2006.

[20] I. Bloch, J. Dalibard, and W. Zwerger. Many-body physics with ultracold gases. 2007.

[21] V. Schweikhard, S. Tung, and E. A. Cornell. Vortex proliferation in the Berezinskii-Kosterlitz-Thouless regime on a two-dimensional lattice of Bose-Einstein condensates. *Phys. Rev. Lett.*, 99(3):030401, 2007.

[22] V. S. Bagnato and D. Kleppner. Bose-Einstein condensation in low-dimensional traps. *Phys. Rev. A*, 44(11):7439–7441, Dec 1991.

[23] N. V. Prokof'ev, O. Ruebenacker, and B. V. Svistunov. Critical point of a weakly interacting two-dimensional Bose gas. *Phys. Rev. Lett.*, 87:270402, 2001.

[24] M. Holzmann and W. Krauth. Kosterlitz-Thouless transition of the quasi two-dimensional trapped Bose gas. *arXiv:0710.5060*, 2007.

[25] D. S. Petrov, M. Holzmann, and G. V. Shlyapnikov. Bose-Einstein condensation in quasi-2D trapped gases. *Phys. Rev. Lett.*, 84:2551, 2000.

[26] D. S. Petrov and G. V. Shlyapnikov. Interatomic collisions in a tightly confined Bose gas. *Phys. Rev. A*, 64:012706, 2001.

[27] F. S. Dalfovo, L. P. Pitaevkii, S. Stringari, and S. Giorgini. Theory of Bose-Einstein condensation in trapped gases. *Rev. Mod. Phys.*, 71:463, 1999.

[28] R. K. Bhaduri, S. M. Reimann, S. Viefers, A. Ghose Choudhury, and M. K. Srivastava. The effect of interactions on Bose-Einstein condensation in a quasi two-dimensional harmonic trap. *J. Phys. B: At. Mol. Opt. Phys.*, 33:3895, 2000.

[29] J. P. Fernández and W. J. Mullin. The two-dimensional Bose-Einstein condensate. *Journal of Low Temperature Physics*, 128:233, 2002.

[30] C. Gies and D. A. W. Hutchinson. Coherence properties of the two-dimensional Bose-Einstein condensate. *Phys. Rev. A*, 70:043606, 2004.

[31] D. S. Petrov, D. M. Gangardt, and G. V. Shlyapnikov. Low-dimensional trapped gases. *J. Phys. IV*, 116:5–44, 2004.

[32] T. P. Simula and P. B. Blakie. Thermal activation of vortex-antivortex pairs in quasi-two-dimensional Bose-Einstein condensates. *Phys. Rev. Lett.*, 96:020404, 2006.

[33] D. R. Nelson and J. M. Kosterlitz. Universal jump in the superfluid density of two-dimensional superfluids. *Phys. Rev. Lett.*, 39:1201, 1977.

[34] V. N. Popov. *Functional Integrals in Quantum Field Theory and Statistical Physics*. D. Reidel Publishing Company, Dordrecht, Holland, 1983.

[35] Y. Kagan, B. V. Svistunov, and G. V. Shlyapnikov. Influence on inelastic processes of the phase transition in a weakly collisional two-dimensional Bose gas. *Sov. Phys. JETP*, 66:314, 1987.

[36] D. S. Fisher and P. C. Hohenberg. Dilute Bose gas in two dimensions. *Phys. Rev. B*, 37:4936, 1988.

[37] U. Al Khawaja, J. O. Andersen, N. P. Proukakis, and H. T. C Stoof. Low dimensional Bose gases. *Phys. Rev. A*, 66(1):013615, Jul 2002.

[38] M. Holzmann, G. Baym, J. P. Blaizot, and F. Laloë. Superfluid transition of homogeneous and trapped two-dimensional Bose gases. *P.N.A.S.*, 104:1476, 2007.

[39] N. V. Prokof'ev and B. V. Svistunov. Two-dimensional weakly interacting Bose gas in the fluctuation region. *Phys. Rev. A*, 66:043608, 2002.

[40] M. Holzmann. Private communication, December 2007.

[41] S. T. Bramwell and P. C. W. Holdsworth. Magnetization: A characteristic of the Kosterlitz-Thouless-Berezinskii transition. *Phys. Rev. B*, 49(13):8811–8814, 1994.